NMR Paramagnetic Relaxation Enhancement: Measurement of an Axial/Equatorial T_1 Ratio for $S = 1$ in the Zero-Field Splitting Limit

Jeremy Miller, Shawn Abernathy, and Robert Sharp*

Department of Chemistry, The University of Michigan, Ann Arbor, Michigan 48109

Received: November 18, 1999; In Final Form: March 6, 2000

An experimental test of one of the central predictions of the theory of paramagnetic enhancement of NMR relaxation rates in solution (the NMR-PRE) for spins $S > {}^1/_2$ is reported. For $S \geq 1$, zero-field splitting (zfs) interactions are present that, when larger than the electronic Zeeman interaction, act to align the spatial quantization of the electron spin motion along the molecule-fixed principal axis system of the zfs tensor. When the zfs energy is comparable to or greater than the Zeeman energy, the NMR-PRE has been predicted theoretically to be a function of the angular variables that specify the orientation of the electron−nuclear interspin vector in the molecular coordinate frame, such that the paramagnetic relaxation enhancement is larger for nuclear spins on the molecular *z*-axis than for nuclear spins in the *x*−*y* plane. The theoretically predicted range for ρ, the ratio of axial/equatorial NMR T_1 relaxation rates, is $1 \leq \rho \leq 4$, the value of unity corresponding to the Zeeman limit ($H_{Zeem} \gg H_{zfs}$); in the zfs limit, ρ is predicted to reach its maximum value, which is significantly greater than unity. The ratio ρ has been determined experimentally for the first time for the axial (H_2O) and equatorial (CH_3) protons of an $S = 1$ complex, $Ni(II)(acac)_2(H_2O)_2$, under conditions that approximate the zfs limit, as was demonstrated from a measurement of the magnetic field dispersion profile of the H_2O proton T_1's. The measured axial/equatorial T_1^{-1} ratio, $\rho_{exp} = 2.2 \pm 0.3$, was significantly greater than unity as expected theoretically. The measured T_1^{-1} ratio was in agreement with the results of spin dynamics simulations carried out by the method of Abernathy and Sharp (*J. Chem. Phys.* **1997**, *106*, 9032).

Introduction

Small concentrations of dissolved paramagnetic metal ions often cause dramatic enhancements of NMR relaxation rates of nuclear spins on ligand and solvent species. This phenomenon, termed the NMR paramagnetic relaxation enhancement or NMR-PRE, has been used widely in studies of the structure, magnetic properties, molecular dynamics, and chemical exchange kinetics of solutions containing paramagnetic solutes.[1−3] The classical theory of the NMR-PRE, due to Solomon[4], Bloembergen[5], and Morgan[6] (SBM theory), can be described as a Zeeman-limit theory since it assumes that the static electron spin Hamiltonian that determines the electron spin quantization and precessional motion is exclusively that of the electronic Zeeman interaction. This picture is almost always appropriate for $S = {}^1/_2$ species, such as Cu(II).

For $S \geq 1$ metal ions, the physical picture is more complex owing to the presence of zero-field splitting (zfs) terms in the electron spin Hamiltonian. Zfs interactions arise from the interplay of electron spin angular momentum with the orbital angular momentum of ground and/or excited electronic states, mediated by spin−orbit coupling. For most $S \geq 1$ oxidation states of the first-row transition metal ions, the static zfs interaction is of roughly comparable magnitude to the electronic Zeeman interaction at ordinary laboratory magnetic field strengths, so that it is often possible to conduct NMR relaxation experiments across a range of Zeeman field strengths corresponding, at low field strength, to the zfs limit, where the zfs hamiltonian is much larger than the Zeeman Hamiltonian ($H_{zfs} \gg H_{Zeem}$), and at high field strength to the Zeeman limit ($H_{Zeem} \gg H_{zfs}$). NMR relaxation data are usually reported as a magnetic field dispersion profile (FDP) of the NMR $T_{1(2)}$ relaxation rate. The shape and magnitude of the FDP are then analyzed by a fit to theory.

The NMR-PRE is fundamentally a measurement of the efficiency of energy transfer between the electron and nuclear spin systems. This phenomenon depends on a resonant coupling between the nuclear (*I*) magnetic moment and the local dipolar magnetic field of the electron spin (*S*). The requirement of energy transfer for a resonant coupling implies a strong dependence of the NMR-PRE on the spatial quantization and precessional (or oscillational) motion of *S*. In the Zeeman limit ($H_S = H_{Zeem}$), the electron spin executes a Larmor precession about the laboratory field axis, in which $\langle S_z \rangle$ is a constant of the motion. In the zfs limit, the electron spin motion is quantized (or polarized) along molecule-fixed coordinate axes. (For simplicity, we restrict a discussion of the zfs limit to $S = 1$, for which the zfs limit energy level diagram is shown in Figure 1.) When the zfs tensor is cylindrical, the electron spin undergoes a precession-like motion in which $\langle S_{\hat{z}} \rangle$ is a constant of the motion, quantized along the unique axis of the molecule-fixed zfs principal axis system (the zfs-PAS; $\hat{x}$, $\hat{y}$, $\hat{z}$), rather than along the laboratory magnetic field. In the corresponding energy level diagram, shown in Figure 1a, the $|\pm 1\rangle$ levels are degenerate. When the zfs tensor contains an orthorhombic component (i.e., when $\hat{x}$ and $\hat{y}$ are chemically distinct), the three Cartesian spin components, $\langle S_r \rangle$ ($r = x, \hat{y}, \hat{z}$), undergo linearly polarized oscillations along the principal axes of the zfs tensor, the oscillation frequencies of which are equal to transition frequencies of the spin system (Figure 1b).

An important consequence of the zfs limit quantization (or polarization) of electron spin motion in the zfs-PAS is that the

* Corresponding author: E-Mail: rrsharp@umich.edu. FAX: 734-647-4865.

10.1021/jp994114c CCC: $19.00
Published on Web 04/14/2000

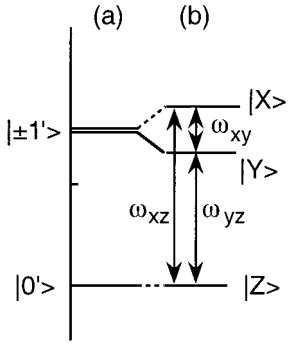

Figure 1. Spin level diagram for $S = 1$ in the zfs limit. In (a), the zfs tensor is cylindrical; the spin eigenstates are circularly polarized along the unique axis of the zfs tensor, and the $|\pm 1'\rangle$ levels are degenerate. In (b) an orthorhombic component E is present; this breaks the $|\pm 1'\rangle$ level degeneracy and forces Cartesian polarizations on the spin eigenfunctions, labeled $|X\rangle$, $|Y\rangle$, and $|Z\rangle$.

NMR-PRE depends, in this limit, on the angular spatial variables that describe the orientation of the $I-S$ interspin vector with respect to the molecular coordinate frame (M-F). Theory predicts that the NMR-PRE, normalized to constant interspin distance, differs markedly for axial and equatorial nuclear locations within the zfs-PAS, such that the distance-corrected axial/equatorial R_{1p} ratio, ρ, lies in the range $1 \leq \rho \leq 4$. In the Zeeman limit, in contrast, the orientation dependence of the NMR-PRE disappears ($\rho = 1$), since in this situation both the electron and nuclear spin motions are quantized along the laboratory magnetic field and are not correlated with the molecular axes. In an isotropic liquid, the spatially averaged $I-S$ dipolar coupling is thus independent of the M-F orientation of the interspin vector.

The dependence of the zfs limit NMR-PRE on the orientation of the $I-S$ vector, although a central prediction of theory, has not previously been studied experimentally. We report here the results of such an investigation. Magnetic-field-dependent T_1 measurements are reported for the "axial" water and "equatorial" methyl ligand protons in the $S = 1$ complex $[Ni(II)(acac)_2(H_2O)_2]$. In this complex, the orientation of the zfs-PAS is determined by the D_{2h} point group symmetry of the Ni(II) coordination sphere. The T_1 data confirm that the distance-corrected zfs limit R_{1p} ratio, $\rho_{exp} = 2.2 \pm 0.3$, is significantly larger than unity in agreement with theoretical prediction.

We also report the results of spin dynamics (SD) simulations[7] of the axial/equatorial R_{1p} ratio. The Ni(II) zfs parameters used in these simulations were obtained from an analysis of the experimental T_1 magnetic field dispersion profile for the water ligand protons. Agreement between experiment and theory was obtained in simulations for which the z-axis and rhombic zfs parameters were $D = 3.2$ cm^{-1} and $E = 0.52$ cm^{-1}, respectively.

Theory

For $S = 1$ in the slow-reorientation, orthorhombic zfs limit, the T_1 NMR-PRE ($\equiv R_{1p}$) is given by[8]

$$R_{1p} = (8/9) r_{IS}^{-6} (\gamma_I \beta_e (\mu_0/4\pi))^2 \{[1 + P_2(\cos\theta_{\hat{z}})]\, j(2\omega_E) + [1 + P_2(\cos\theta_{\hat{x}})]\, j(\omega_D + \omega_E) + [1 + P_2(\cos\theta_{\hat{y}})]\, j(\omega_D - \omega_E)\} \quad (1)$$

γ_I is the nuclear magnetogyric ratio, β_e is the Bohr magneton, r_{IS} is the $I-S$ interspin distance, and μ_0 is the magnetic permeability of free space. The functions $1 + P_2(\cos\theta_{\hat{r}})$ ($r = \hat{x}, \hat{y}, \hat{z}$) describe the dependence of R_{1p} on the angular variables that specify the orientation of the nuclear spin in the molecular coordinate frame: $\theta_{\hat{r}}$ is the polar angle of the $I-S$ interspin vector with respect to the $\hat{r}$th molecular-frame Cartesian axis. $j(\omega)$ is the spectral density function

$$j(\omega) = \frac{\tau_S}{1 + \omega^2 \tau_S^2} \quad (2)$$

and τ_S is the electron spin decay time. Equation 2 assumes slow Brownian reorientation, i.e., that the reorientational correlation time $\tau_R^{(2)} \gg \tau_S$. ($\tau_R^{(2)}$ is describes reorientation of a molecule-fixed second-rank tensor and is related to $\tau_R^{(1)}$, the reorientational correlation time for a molecule-fixed vector by $\tau_R^{(2)} = \tau_R^{(1)}/3$.)

The calculation of R_{1p} in the presence of rapid Brownian reorientation was carried out by spin dynamics (SD) simulation. The SD algorithms, which are described elsewhere,[7] use the quantum mechanical equations of motion of the spin variables in conjunction with a classical simulation of molecular Brownian reorientation to calculate the time correlation functions (TCF) of the electron spin. The algorithms generate the TCF's as a statistical mechanical average in the time domain by averaging over typically 7000 spin trajectories, each composed of 50 to several thousand time points as required to define temporal fluctuations in the TCF. This degree of averaging gives random noise of approximately $\pm 3\%$ in the simulated R_{1p}'s.

Equation 1 describes the zfs limit NMR-PRE, which is a function of the angular variables ($\theta_{\hat{x}}$, $\theta_{\hat{y}}$, $\theta_{\hat{z}}$) specifying the orientation of the interspin vector in the molecular coordinate frame. An experimental test of the angular dependence described by equation 1 is the objective of this study. In the Zeeman limit, the electron spin motion is quantized along the laboratory, rather than molecular, axes, and this angular dependence is not present. The Zeeman limit expression that corresponds to eq 1 is[4-6]

$$R_{1p} = \left(\frac{2}{15}\right)\left(\frac{\gamma_I g_e \beta_e}{r_{IS}^3}\right)^2 \left(\frac{\mu_0}{4\pi}\right)^2 S(S+1)\,[3j(\omega_I) + j(\omega_S - \omega_I) + 6j(\omega_S + \omega_I)] \quad (3)$$

This expression (unlike eq 1) can be written in a form valid for fast as well as slow Brownian reorientation by replacing τ_S in eq 2 by the dipolar correlation time, τ_d

$$\tau_d^{-1} = (\tau_R^{(2)})^{-1} + \tau_S^{-1}$$

The electron spin relaxation time, τ_S, in general exhibits magnetic field dependence when the spin levels of S depend on the Zeeman energy. This behavior could become important in the SD analysis of the proton fdp data that was used to determine the values of the spin parameters, E and τ_S, and thus its influence needs to be considered. The magnetic field dependence of τ_S is a rather complex problems. To summarize briefly, τ_S^{-1} is the sum of three distinct mechanistic contributions arising from collisional,[6,9] reorientational,[10] and vibrational[11] modulation of the zfs tensor:

$$\tau_S^{-1} = \tau_{S,c}^{-1} + \tau_{S,R}^{-1} + \tau_{S,v}^{-1} \quad (4)$$

The reorientational contribution, including its magnetic field dependence, is calculated directly by the SD algorithms described above. No parametrization of $\tau_{S,R}$ is required in addition to the static zfs parameters (D, E) and $\tau_R^{(2)}$. $\tau_{S,c}$ and $\tau_{S,v}$ must be parametrized independently; they are unknown on an a priori basis, in both relative and absolute terms, because of large uncertainties in the coupling constants and correlation times that determine these quantities. $\tau_{S,v}$ is independent (or very

nearly so) of the Zeeman field strength.[11,12] $\tau_{S,c}$ is independent of the Zeeman field in the low-field region but lengthens when the Zeeman energy is large enough that the sdf's that determine $\tau_{S,c}$ become magnetic-field-dependent owing to field dependence in the level splittings.[6] When the field dependence introduced by $\tau_{S,c}^{-1}$ into eq 4 is negligible, the use of a single field-independent relaxation parameter is appropriate: $(\tau_S')^{-1} = \tau_{S,v}^{-1} + (\tau_{S,c})_0^{-1}$, where $(\tau_{S,c})_0$ is the low-field value of $\tau_{S,c}$. It is clearly advantageous to work in the regime where $\tau_{S,c}$ is field-independent, since the description of τ_S then involves a single unknown parameter (τ_S'), rather than three ($\tau_{S,v}$, $(\tau_{S,c})_o$, and the collisional correlation time, τ_v).

As described below, calculations of $\tau_{S,c}$ were also undertaken in which the field dependence of this quantity was described using a modification of Westlund's expression (ref 13, eq 63) for τ_{S2} in which the zfs limit level splittings were replaced by spatially averaged field-dependent level splittings determined by diagonalizing the spin Hamiltonian. This procedure accounts approximately for the field dependence of the spin levels as well as of $\tau_{S,c}$ in the vicinity of the zfs limit.

Experimental Section

$Ni(acac)_2(H_2O)_2$ (acac = 2,4-pentanedionato) was synthesized by the method of Charles and Pawlikowski.[14] The blue-green complex was characterized by IR, UV−vis, and magnetic susceptibility measurements, which were in agreement with literature. A solution was prepared in H_2O and diluted 1:3 in 2,4 dioxane, and a UV−vis spectrum was obtained. From the literature value of $\epsilon_{max} = 5.00$ at 640 nm,[15] the concentration of the complex was determined to be 20.9 mM. A 200 μL NMR sample of this solution and a water blank were degassed by five freeze−pump−thaw cycles and sealed under vacuum.

The intermolecular contribution to R_{1p} was measured using $Ni(acac)_2(H_2O)_2$ solutions prepared in mixed dioxane−$H_8/^2H_2O$ solvent containing 5, 10, 15, and 20% dioxane. The dioxane ^1H T_1 was measured as a function of dioxane concentration and extrapolated back to 0% dioxane. The extrapolated R_{1p} of dioxane, corrected for the difference in self-diffusion coefficients of aqueous dioxane and water, gives the intermolecular R_{1p} of the water protons. The correction for the difference in self-diffusion coefficients was small (5%) since the translational dipolar correlation time is primarily determined by τ_S rather than by diffusional motion.

The R_1 magnetic field dispersion profile (fdp) of the solvent peak was measured between 0.14 and 1.4 T using a home-built variable-field NMR relaxation spectrometer. T_1 was measured by the phase-shifted triplet sequence,[16] $(\pi)_0-[\tau_d-(\pi/2)_0-\tau_{tr}-(\pi)_\pi-\tau_{tr}-(\pi/2)_0]_n$, in which an initial inverting pulse is followed by a train of pulse triplets. Each triplet samples the total magnetization by means of a $\pi/2$-pulse, then refocuses it with a phase-shifted π-pulse, and restores the magnetization along z with a second $\pi/2$-pulse. In order that the sampling triplet cause little perturbation of the decaying magnetization, τ_{tr} is set to be short compared to τ_d, typically, $\tau_{tr} < 0.01\tau_d$. For strong signals such as solvent, the repeatability of T_1 determinations on a given sample is typically ±1% or better. The temperature was held at 24.0 ± 0.2 °C by a stream of dry nitrogen and checked periodically with a calibrated thermistor in a dummy sample.

Results

A 200 MHz high-resolution proton NMR spectrum of a saturated $Ni(acac)_2(H_2O)_2$ solution in D_2O (99.96 atom % ^2H) is shown in Figure 2. The spectrum contained three peaks, assigned to methyl, methine, and water protons (the latter due to exchangeable protons from the complex and to residual protons in the ^2H_2O solvent), the latter assigned by sequential addition of H_2O. The methyl and water integrals were in an approximate 1:1 ratio, although spectral overlap prevented precise integration. The methine peak appears upfield at approximately −13 ppm and shows <1:20 integrated ratio with the methyl peak, indicating that the methine protons undergo extensive exchange with ^2H from the solvent. The methyl proton peak has a line width approximately 12 times greater than that of the water peak. The methyl proton R_1 was measured at 10.38 MHz (0.24 T) and 24.0 ± 0.2 °C using the phase-shifted triplet sequence as described above. These measurements sampled a combined signal of all three proton peaks, and accordingly the decay was strongly nonexponential (Figure 3), owing to the fast-relaxing methyl component and slowly relaxing water component. The methine peak contributes <3% of the signal and was ignored. The water component was relatively slowly relaxing, and its R_1 was measured in a separate experiment conducted using relatively long sampling intervals (>120 ms), giving $R_{1p} = 2.7\ s^{-1}$. The water and methyl peaks have R_1 values that differ by a factor of 17 and were easily separable. The water signal, which was taken to be the component remaining at $t >$ 120 ms, was extrapolated to zero time using the measured water proton R_1 and subtracted from the total, leaving the methyl signal

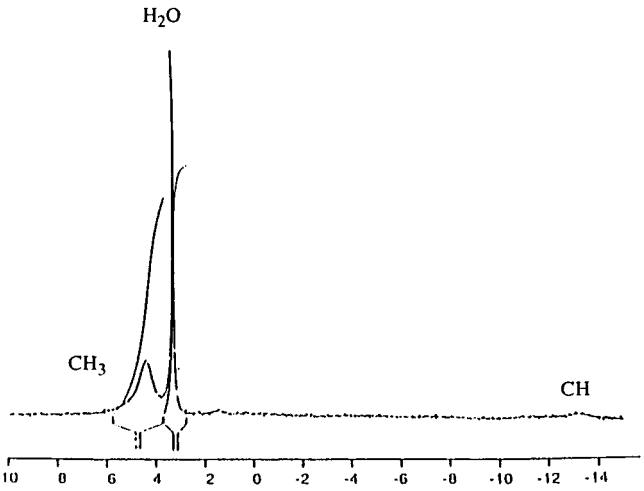

Figure 2. High-resolution proton NMR spectrum of a saturated solution of $Ni(acac)_2(H_2O)_2$ in D_2O at 200 MHz.

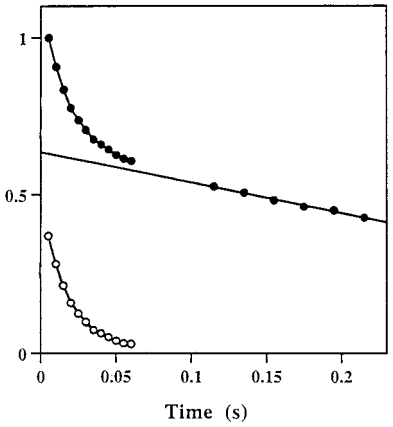

Figure 3. Plot of the total proton signal (methyl + water) measured at 0.24 T using the triplet sequence (solid circles). The methyl signal (open circles) was calculated by subtracting the water signal (solid line) from the total.

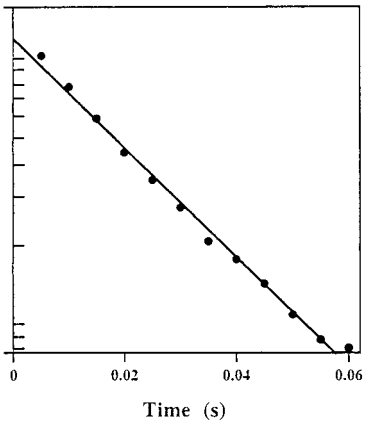

Figure 4. Plot of ln(signal) (arbitrary units) vs time (s) for the methyl proton resonance in $Ni(acac)_2(H_2O)_2$. R_1 for the methyl proton resonance is 47.2 s^{-1}.

(open circles). Figure 4 shows the plot of ln(signal) vs time for the methyl protons, from which the value $R_1 = 47 \pm 3$ s^{-1} was obtained.

In a separate experiment using a 21 mM sample of $Ni(acac)_2(H_2O)_2$ prepared in protonated solvent, the R_1 for the water protons was measured at 10.38 MHz and found to be 2.13 ± 0.02 s^{-1} at 24.0 ± 0.2 °C. The intermolecular R_{1p} contribution was measured in separate experiments using solutions prepared in mixed dioxane/^2H_2O solvents as described above and found to be 0.18 ± 0.01 s^{-1}. The intermolecular R_{1p} contribution was also computed theoretically by SD simulation. The calculation used a distance of closest approach of dioxane protons to the Ni(II) ion that was estimated from molecular dynamics simulations using the commercial modeling and dynamics program Cerius[2] (Biosym/MSI, Inc). The calculated intermolecular contribution, $R_{1p}' = 0.17$ s^{-1}, was in good agreement with experiment.

After correcting for the intermolecular contribution and the diamagnetic background (0.306 ± 0.003 s^{-1}), the intramolecular contribution to R_{1p} was 1.72 ± 0.08 s^{-1}. R_{1m} ($\equiv T_{1m}^{-1}$), the relaxation rate of the water protons in the metal coordination sphere, was calculated from the Luz−Meiboom equation[17]

$$R_{1p} = \frac{f_m}{T_{1m} + \tau_m}$$

where f_m is the (bound/free) mole ratio of the water ligand. Assuming rapid chemical exchange of water protons ($\tau_m \ll T_{1m}$), $R_{1m} = 2200 \pm 200$ s^{-1}. The experimental axial/equatorial R_1 ratio computed before accounting for the difference in Ni−H distances is thus 47 ± 5.

This value was corrected for the difference in axial and equatorial $I-S$ interspin distances using results from X-ray[18] and neutron[19] diffraction studies. The Ni−H distance in aquated Ni(II) cation has been determined by neutron diffraction in 2 M $NiCl_2$ to be 2.65 Å. Scaling this distance to account for the larger Ni−water oxygen distance in $Ni(acac)_2(H_2O)_2$ ($r_{H_2O} = 2.140$ Å[18] relative to the Ni−O distance ($r = 2.04$ Å) in the aquated Ni^{2+} cation[19]) gives the value $r_{IS} = 2.78$ Å for the axial Ni−H distance. Using the measured Ni−O from X-ray diffraction and the Ni−H distance from neutron diffraction in conjunction with the O−H bond distance, 0.94 Å, in water, the O−Ni−H angle, which equals the polar angle $\theta_{\hat{z}}$, is 17° (this angle is fixed by the Ni−O, Ni−H, and O−H distances). From the X-ray crystal structure of the complex, the average Ni−C distance for the methyl carbons is 4.5 Å. Assuming tetrahedral

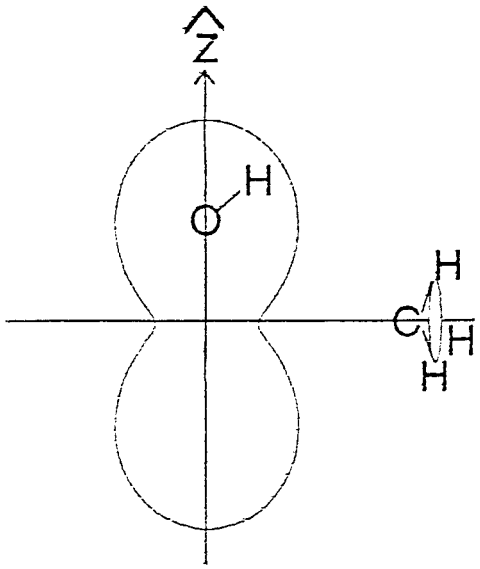

Figure 5. Positions of the water and methyl protons of $Ni(acac)_2(H_2O)_2$ in the molecular coordinate frame. Scaled drawing shows the correct polar angles and relative $I-S$ interspin distances. Superimposed is a plot of the function $1 + P_2(\cos \theta_{\hat{z}})$.

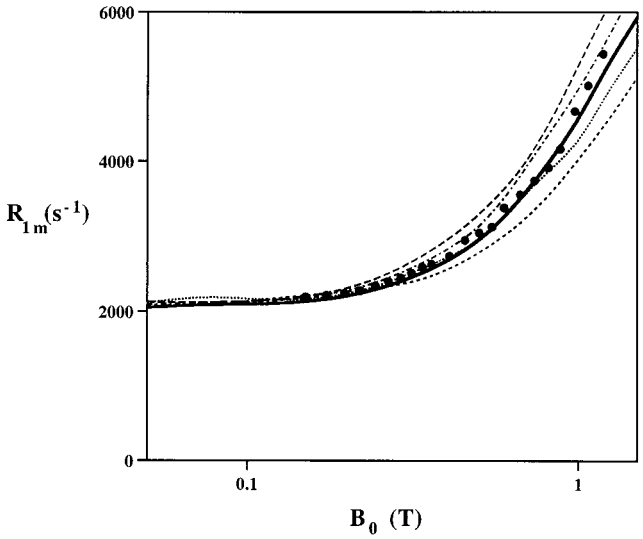

Figure 6. Comparison of experimental (solid circles) and spin dynamics simulations of the FDP for $Ni(acac)_2(H_2O)_2$. Each curve was computed assuming a pair of values, E and τ_S', selected to fit the low-field limiting data. The following parameter sets were used: 55 cm^{-1}, 15 ps (small dashes), 0.53 cm^{-1}, 17 ps (dots), 0.52 cm^{-1}, 19 ps (solid bold), 0.50 cm^{-1}, 22 ps (dot−dash), 0.49 cm^{-1}, 24 ps (large dashes). Other parameters used in the simulations were $r_{IS} = 2.78$ Å, $D = 3.2$ cm^{-1}, $\theta = 0.293$ rad, and $\tau_R^{(2)} = 77$ ps.

bond angles, the methyl Ni−H distance is 4.65 Å, and $\cos^2(\theta_{\hat{z}})$ for the methyl protons is 0.02. Figure 5 shows a drawing of the complex scaled to show the relative Ni−H distances and molecular polar angles. Superimposed on the drawing is a plot of the function $1 + P_2 \cos(\theta_{\hat{z}})$, which describes the angular variation of the NMR relaxation efficiency (see below). Using these distances, the distance-corrected axial/equatorial R_1 ratio is $\rho_{exp} = 2.2 \pm 0.3$.

The magnetic field dispersion profile for the water proton R_{1p} was measured between 6 and 63 MHz (Figure 6). The FDP exhibits the characteristic magnetic field dependence[20−24] of orthorhombic Ni(II) ($S = 1$) spin systems, namely, a profound rise in R_{1p} with increasing Zeeman field strength in the range of 0.3−1.5 T.

Data Analysis

The theoretical axial/equatorial R_{1p} ratio was calculated using spin dynamics simulation techniques. The water proton FDP for $Ni(acac)_2(H_2O)_2$ was measured as described above and analyzed to provide the physical parameters used in the spin dynamics simulations. The simulations depend on seven physical parameters, which include the three structural parameters, r_d, θ, and ϕ, specifying the length and orientation of the $I-S$ interspin vector; the reorientational correlation time, $\tau_R^{(2)}$; and the three electron spin parameters, D, E, and τ_S. Values of the structural parameters, θ and r_d, were taken from diffraction studies as described above. Calculated values of R_{1m} for the bound water protons are nearly independent of the azimuthal angle ϕ at the relatively small polar angle, $\theta = 17°$, of the water protons, and thus ϕ was taken to be 0. $\tau_R^{(2)}$ for the complex was estimated from the Debye equation[25] to be 77 ps in water at 24 °C.

Among the electron spin parameters, the form of the low-field FDP depends relatively sensitively on E and τ_S, and much less sensitively[26] on D except when D is relatively small, roughly $D < 5$ cm^{-1}. The relative insensitivity to D is due to the fact that the NMR-PRE is influenced more strongly by the small splitting, $2\omega_E$, than by the large splittings, $\omega_D \pm \omega_E$. E and τ_S were determined by a procedure described previously. Initial fits to the low-field data were first performed to find pairs of E and τ_S values that satisfactorily fit the low-field limiting R_{1p} data at a specified value of D. Then series of pairs of τ_S and E values that fit the low-field data were used in spin dynamics simulations of the full R_1 FDP. This procedure gave values of $\tau_S = 19 \pm 2$ ps and $E = 0.52 \pm 0.02$ cm^{-1} at a fixed value of $D = 3.2$ cm^{-1}; this value of D gave the best agreement between observed and calculated R_{1p} ratios (see below). The sensitivity of the fits to variations in E and τ_S at constant D is illustrated by Figure 6, which shows a series of five curves bracketing the best fit at $D = 3.2$ cm^{-1}. Uncertainties in E and τ_S were estimated by bracketing the data in this way.

These simulations assumed a field-independent parameter τ_S' in eq 4. This assumption provided good agreement between theory and experiment as shown in Figure 6. The assumption that $\tau_{S,c}$ is effectively magnetic-field-independent over the experimental range of field variation was examined in calculations of $\tau_{S,c}$ in which the field dependence was described by a modification of Westlund's expression for τ_{S2}, in which the zfs limit energies were replaced by the spatially averaged field-dependent level splittings determined by diagonalization of the spin Hamiltonian. The parameters in Westlund's expression were taken to be $\Delta_t^2 = 0.875$ cm^{-2} and $\tau_v = 3$ ps; these values give a τ_S' consistent with the low-field fdp data (Figure 6). A plot of $\tau_{S,c}$ vs B_0 is shown in Figure 7. The change in $\tau_{S,c}$ was small, about 3%, across the range of experimental data supporting the use of a field-independent relaxation parameter τ_S' in the analysis.

The theoretical axial/equatorial R_{1p} ratio, ρ_{calc}, was computed by spin dynamics simulation techniques. The results of these simulations, in which ρ_{calc} was computed as a function of D with other parameters, as given in the figure legend, are shown in Figure 8. ρ_{calc} increased with increasing D up to $D \approx 6$ cm^{-1} and was essentially constant at larger values of D. The measured value of $\rho_{exp} = 2.2$, shown as a solid circle with error bars, matches the calculated value when $D = 3.2 \pm 0.8$ cm^{-1}. This value of D is well within the reported range of $2-10$ cm^{-1} for tetragonally distorted Ni(II) complexes that have been measured previously by EPR,[27] calorimetry,[28] and temperature-dependent magnetic susceptibility[29] measurements.

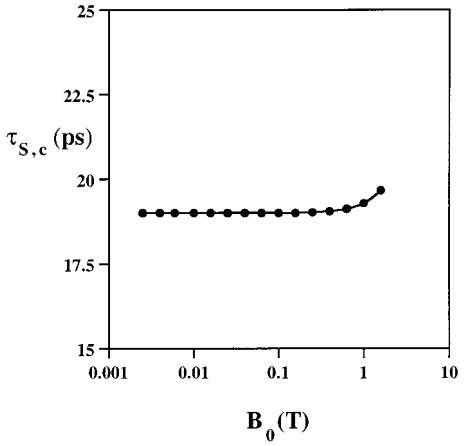

Figure 7. Plot of the field dependence of $\tau_{S,c}$ calculated using Westlund's zfs limit expression,[13] modified to describe the magnetic field dependence of the spin levels as described in the text. Physical parameters of the calculation are $\Delta_t^2 = 0.875$ cm^{-2}, $\tau_v = 3$ ps.

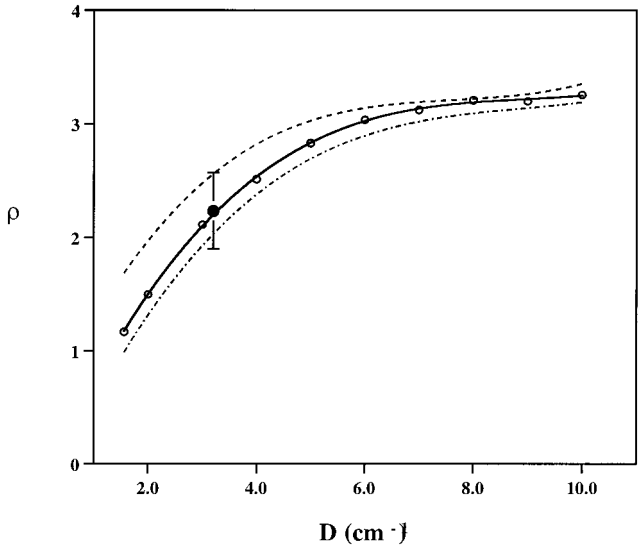

Figure 8. Computed axial/equatorial R_1 ratios as a function of the ZFS parameter D. Results of spin dynamics simulations are shown at three values of the azimuthal angle ϕ: $\phi = \pi/4$ (solid), $\phi = 0$ (dashes), $\pi/2$ (dot−dash). Other parameters used in the simulations are in the legend of Figure 6 (with $\tau_S = 19$ ps, $E = 0.52$ cm^{-1}, and $B = 0.244$ T), The experimental axial/equatorial ratio is shown as a solid circle with error bars.

The solid curve of Figure 8 was calculated assuming an azimuthal angle $\phi = \pi/4$ for the methyl protons. In the crystal structure, the methyl carbons lie very close to the $\phi = \pi/4$ axis, and the average azimuthal angle for the methyl protons is close to $\phi = \pi/4$. To examine the sensitivity of the analysis to variations in ϕ, simulations were also performed at the limiting values, $\phi = 0$ and $\phi = \pi/2$, and the results are shown as dashed lines in Figure 8. These simulations confirmed that the uncertainty introduced into ρ_{calc} by uncertainty in the methyl proton ϕ-value is small.

Discussion

Table 1 compares the calculated and experimental axial/equatorial R_1 ratios for $Ni(acac)_2(H_2O)_2$ in aqueous solution. We conclude the following: (1) the measured zfs limit axial/equatorial R_1 ratio, $\rho_{exp} = 2.2$, is substantially larger than the Zeeman limit value of unity as predicted theoretically;[30,31] (2) ρ_{exp} is in the theoretically predicted range of $1 \leq \rho_{calc} \leq 4$; (3)

TABLE 1: Comparison of Calculated and Experimental Axial/Equatorial R_{1p} Ratios[a]

theory	ratio
(1) Zeeman (SBM) limit theory	1
(2) uniaxial ZFS limit[8]	3.4
(3) SD simulation[7]	
$D = 3.2\ cm^{-1}$, $E = 0.52\ cm^{-1}$	
$\tau_S' = 19$ ps, $\tau_R^{(2)} = 77$ ps	
$\phi = 0$	2.4
$\phi = 45$	2.2
$\phi = 90$	1.8
experimental ZFS limit	2.2 ± 0.3

[a] Spin dynamics simulations were performed by the method of ref 7.

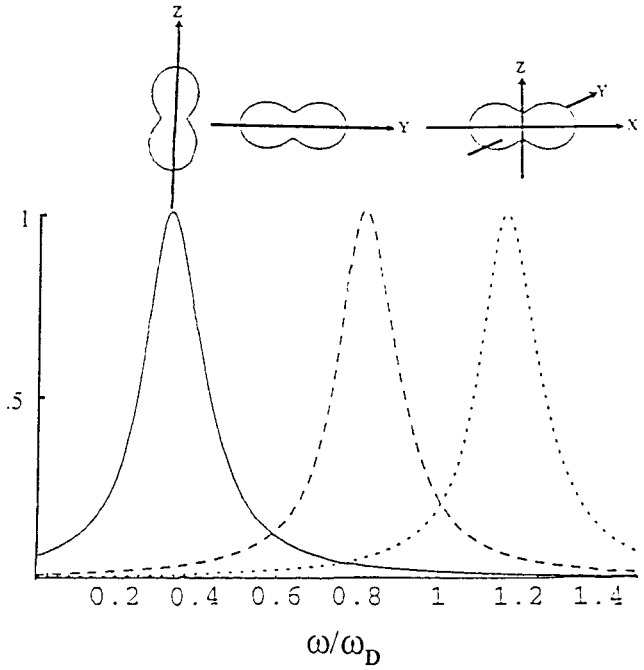

Figure 9. Dipolar power density vs frequency associated with $\langle S_x \rangle$ (dots), $\langle S_y \rangle$ (dashes), and $\langle S_z \rangle$ (solid). The plots above represent the angular functions $1 + P_2(\cos\ \theta_r)$ associated with each Cartesian polarization of the spin motion.

the measured axial/equatorial ratio, ρ_{exp}, was in agreement with a theoretical value of ρ calculated by spin dynamics simulations. Parameters used in the SD simulations were measured from an independent experiment involving an analysis of the T_1 magnetic field dispersion profile of the complex.

The overall uncertainty in ρ_{exp} is estimated to be ±15%. The systematic and random error of the NMR measurements is determined by the methyl proton R_1, for which the uncertainty is estimated to be ±4%. For the water protons, where the S/N ratio is much higher, the uncertainty is ±1%. The experimental distance ratio of the methyl and water protons enters the analysis as an inverse sixth power and is the largest source of experimental uncertainty. The uncertainty in the X-ray Ni−O distance for the water oxygen is approximately ±1% or ±0.03 Å.[18] The uncertainty in the Ni−H distance for the water protons is estimated to be twice as large or ±0.06 Å (±2%). The uncertainty in the Ni−C(methyl) distance is <1%. The overall uncertainty in the distance-corrected axial/equatorial R_1 ratio is thus estimated to be ±15% or $\rho_{exp} = 2.2 \pm 0.3$. This value is significantly above the Zeeman limit value of unity.

The physical origin of an axial/equatorial ratio greater than unity will be described with reference to Figure 9. The efficiency of electron spin−nuclear spin energy transfer, which is measured by the NMR relaxation rate, R_{1p}, depends on the Fourier transforms, evaluated at the nuclear Larmor frequency, of the time correlation functions, $G_r(t) = \langle S_r(0) \cdot S_r(t) \rangle$ ($r = x, y, z$), of the electron spin components, $S_r(t)$. In the orthorhombic zfs limit, the electron spin motion is quantized (or polarized) along the zfs principal axes in the molecular frame. $G_{\hat{x}}(t)$ has nonvanishing matrix elements only between the spin eigenstates $|Y\rangle$ and $|Z\rangle$ and oscillates at the transition frequency, $\omega_{YZ} = \omega_D + \omega_E$. Similarly, $G_{\hat{y}}(t)$ has nonvanishing matrix elements only between the spin eigenstates $|X\rangle$ and $|Z\rangle$ and oscillates at the transition frequency, $\omega_{XZ} = \omega_D - \omega_E$. $G_{\hat{z}}(t)$ has nonvanishing matrix elements only between the spin eigenstates $|X\rangle$ and $|Y\rangle$ and oscillates at the transition frequency, $\omega_{XY} = 2\omega_E$. NMR relaxation efficiency depends on the dipolar power density at low frequency, specifically at ω_I for T_1, and, for T_2, at frequencies of 0 and ω_I. When $\omega_E \ll \omega_D$, the preponderance of the low-frequency dipolar power is produced by $G_{\hat{z}}(t)$, and thus the effects of $G_{\hat{x},\hat{y}}(t)$ are small, often negligible. This situation is illustrated by the dipolar power density plots in Figure 9.

The local dipolar coupling energy associated with each $G_r(t)$ is proportional to the spatial function $1 + P_2(\cos\ \theta_r)$, where $P_2(x)$ is the second-order Legendre polynomial and θ_r is the angle between the $I-S$ interspin vector and the rth Cartesian coordinate axis. This spatial function describes the mean-squared dipolar field produced by a classical dipole oriented along the rth Cartesian axis.[8] Contour plots of this function, oriented along $\hat{x}$, $\hat{y}$, and $\hat{z}$, are shown in Figure 9. Because most of the low-frequency dipolar power density arises from $G_{\hat{z}}(t)$, axial nuclear positions are more strongly relaxed than equatorial positions at constant interspin distance. The maximum predicted zfs limit, the distance-corrected axial/equatorial R_{1p} ratio is $\rho = 4$, determined by the angular function $1 + P_2(\cos\ \theta_{\hat{z}})$ when the dipolar power produced by the transverse components, $G_{\hat{x},\hat{y}}(t)$, is negligible. In practical cases, the R_{1p} ratio is reduced below 4 owing to the effects of Brownian reorientation as well as the influence of the transverse TCF's.

When the transverse TCF's contribute significantly to R_1, $\hat{x}-\hat{y}$ anisotropy of relaxation efficiency will be present owing to the larger influence of $G_{\hat{y}}(t)$ relative to $G_{\hat{y}}(t)$. (We have defined E as positive, corresponding to a choice of $\hat{x}$ and $\hat{y}$ axes such that the energy of $|Y\rangle$ is between that of $|X\rangle$ and $|Z\rangle$). The $\hat{x} - \hat{y}$ anisotropy can be described in terms of the angular functions $1 + P_2(\cos\ \theta_{\hat{x}})$ and $1 + P_2(\cos\ \theta_{\hat{y}})$, each weighted by the low-field dipolar power density associated with $G_{x(y)}(t)$. The effects of $\hat{x} - \hat{y}$ anisotropy are probably insignificant in the above analysis, since the equatorial methyl protons of $[Ni(acac)_2(H_2O)_2]$ lie close to the $\varphi = \pi/4$ axis in the zfs-PAS. However, it is interesting to consider the effect that $\hat{x} - \hat{y}$ anisotropy would have on ρ_{calc} in a hypothetical complex where the equatorial nuclear spin were positioned along $\varphi = 0$ or $\pi/2$. These calculations are shown as dashed lines in Figure 8. Across the full range of physical variation in φ, $0 \le \varphi \le \pi/2$, the influence of $\hat{x} - \hat{y}$ anisotropy is modest, with the $\hat{y}$-direction more strongly relaxing than the $\hat{x}$-direction for the reasons described above and in Figure 9.

Acknowledgment. This research was supported by the U.S. National Science Foundation in the form of a research grant, CHE-9423351.

References and Notes

(1) Dwek, R. A. *NMR in Biology*; Academic: London, 1977.
(2) Banci, L.; Bertini, I.; Luchinat, C. *Nuclear and Electron Relaxation*; VCH Publishers: Weinheim, Germany, 1991.
(3) Bertini, I.; Luchinat, *C. Coord. Chem. Rev.* **1996**, 150.

(4) Solomon, I. *Phys. Rev.* **1955**, *99*, 555.
(5) Bloembergen, N. *J. Chem. Phys.* **1957**, *34*, 842.
(6) Bloembergen, N.; Morgan, L. O. *J. Chem. Phys.* **1961**, *34*, 842.
(7) Abernathy, S. M.; Sharp, R. R. *J. Chem. Phys.* **1977**, *106*, 9032.
(8) Sharp, R. R.; Abernathy, S. M.; Lohr, L. L. *J. Chem. Phys.* **1997**, *107*, 7620.
(9) M. Rubinstein, M.; Baram, A; Luz, Z. *Mol. Phys.* **1971**, *20*, 67.
(10) Carrington, A.; Luckhurst, G. R. *Mol. Phys.* **1964**, *8*, 125.
(11) Al'tshuler, S. A.; Valiev, K. A. *Soviet Phys. JETP* **1959**, *35*, 661.
(12) Westlund, P.-O.; Benetis, N.; Wennerstrom, H. *Mol. Phys.* **1987**, *61*, 177.
(13) Westlund, P. O. *J. Chem. Phys* **1998**, *108*, 4945.
(14) Charles, R. G.; Pawlikowski, M. A. *J. Phys. Chem.* **1958**, *62*, 440.
(15) Cotton, F. A.; J. P. Fackler, J. P. *J. Am. Chem Soc.* **1961**, *83*, 2818.
(16) Haddy, A. E.; Frasch, W. D.; Sharp, R. R. *Biochemistry* **1985**, *24*, 7926.
(17) Luz, Z.; Meiboom, S. *J Chem. Phys.* **1965**, *40*, 2686.
(18) Montgomery, H.; Lingafelter, E. C. *Acta Crystallogr.* **1964**, *17*, 1481.
(19) Powell, D. H. *J. Phys: Condens. Matter* **1989**, *1*, 8721.
(20) Benetis, N.; Kowalewski, J.; Nordenskiold, L. *J. Magn. Reson.* **1984**, *58*, 282.
(21) Westlund, P.-O.; Larsson, P. T. *Acta Chem. Scand.* **1991**, *45*, 11.
(22) Larsson, T.; Westlund, P.-O.; Kowalewski, J.; Koenig, S. H. *J. Chem. Phys.* **1994**, *101*, 1116.
(23) Abernathy, S. M.; Miller, J. C.; Lohr, L. L.; Sharp, R. R. *J. Chem. Phys.* **1998**, *109*, 4035.
(24) Reference 2, pp 134−136.
(25) Abragam, A. *The Principles of Nuclear Magnetism*; Oxford University: London, 1961; Chapter 8.
(26) Abernathy, S. M.; Sharp, R. R. *J. Phys. Chem.* **1997**, *101*, 3692.
(27) Griffiths, J. H. E.; Owen, J. *Proc. R. Soc. London* **1952**, *213*, 473.
(28) Klaaijsen, F. W.; Reedijk, J.; Witteveen, H. T. *Z. Naturforsch.* **1972**, *27A*, 1532.
(29) Reedijk, J.; Witteveen, H. T.; Klaaijsen, F. W. *J. Inorg. Nucl. Chem.* **1973**, *35*, 3439.
(30) Sharp, R. R. *J. Chem. Phys.* **1990**, *93*, 6921.
(31) Sharp, R. R. *J. Chem. Phys.* **1993**, *98*, 912; **1993**, *98*, 250.